Available online at www.sciencedirect.com
SCIENCE DIRECT
Journal of Power Sources 158 (2006) 378–384
JOURNAL OF POWER SOURCES
www.elsevier.com/locate/jpowsour

Innovative design to improve the power density of a solid oxide fuel cell

P.A. Ramakrishna *, Shi Yang, C.H. Sohn

School of Mechanical Engineering, Kyungpook National University, Daegu 702-701, South Korea

Received 29 August 2005; received in revised form 30 September 2005; accepted 3 October 2005
Available online 15 December 2005

Abstract

This paper explores the possibility of improving the power density of a solid oxide fuel cell (SOFC). A three-dimensional computational model (CFD-ACE package), with the relevant sub-models was used for the study. The performance of the SOFC was examined with a thin wall, which splits the inlet section and runs up to half the length of the flow channels. The results obtained with this (thin-walled) geometry were consistently better than those obtained with plain geometry (without the thin wall). The polarization characteristics of the thin-walled geometry indicated that the maximum power density obtained was 1.18 W cm^{-2} at an efficiency of around 60%. The corresponding values of maximum power density and the efficiency at which it was obtained for a plain geometry were 0.88 W cm^{-2} and 50%, respectively. The enhanced performance of the thin-walled geometry was attributed to a better distribution of the reactants along the length of the SOFC. Studies were also conducted to verify the performance of the thin-walled geometry over a wide range of inlet mass flow rates. They revealed a superior performance of the thin-walled geometry compared to the plain geometry. At lower inlet mass flow rates, the difference between the two in performance was small, but at higher inlet mass flow rates the difference in performance was significant.

Keywords: SOFC; Modeling; Power density

1. Introduction

Following the discovery by Nernst in 1899 that zirconia can act as an oxygen carrier, a practical solid oxide fuel cell (SOFC) was developed by Baur and Pries in 1937. A good historical perspective of the development of SOFC can be found in [1]. Recently, major consortiums like Siemens–Westinghouse [2,3], BMW Delphi [4], Rolls Royce [5] have all identified the low power density of SOFC as an area for improvement, if the future SOFC systems are to become financially viable following the target set by the Solid State Energy Conversion Alliance (SECA) [6].

A brief review of some of the past efforts to enhance the power density of a SOFC is presented here. Li et al. [7] have proposed a new design for the gas distributor in fuel cells, which improves the power density of a SOFC. In their design, a large number of small current collectors surrounded by a small reactive area have been used to obtain the enhanced power density. They claim that through their new design the access area of reactants to the electrode/electrolyte layer has led to an enhanced mass transfer and higher power density. They have demonstrated the viability of their new design through experiments on PEM (proton exchange membrane) fuel cells, wherein they claim to have obtained a 40% improvement in power density for a single fuel cell.

Sung et al. [8] and Takashi et al. [9] have reported obtaining improved power density in SOFCs by using a new material. Sung et al. [8] have modified the Ni/yttria-stabilized zirconia (YSZ) cermet anode by coating with a samaria-doped ceria (SDC, $Sm_{0.2}Ce_{0.8}O_2$) sol within the pores of the anode. They report a 50% increase in power density along with a smaller degradation in performance over time. Takashi et al. [9] report an increased maximum power density (from 161 to 213 mW cm^{-2}) using an yttria-stabilized zirconia solid electrolyte with a 25 wt.% $Ce_{0.8}Gd_{0.2}O_{1.9}$ (GDC)-containing Ni anode and a 15 wt.% MnO_2-containing $La_{0.8}Sr_{0.2}MnO_3$ cathode.

Bharadwaj et al. [2] and Lu et al. [10] have performed computational studies on the flattened tubular SOFC designed

* Corresponding author. Tel.: +91 44 2257 4018; fax: +91 44 2257 4002.
E-mail address: rama@ae.iitm.ac.in (P.A. Ramakrishna).

0378-7753/$ – see front matter © 2005 Elsevier B.V. All rights reserved.
doi:10.1016/j.jpowsour.2005.10.030

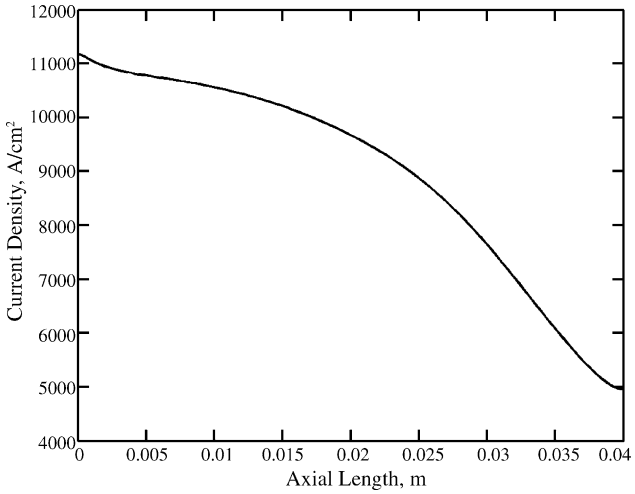

Fig. 1. The current density variation along the axial length of the SOFC at $y = 0$ and $z = 0$ at a voltage of 0.73 V.

by Siemens–Westinghouse Corporation. In these studies, it is reported that a flattened SOFC delivers a higher power density than the conventional tubular SOFC. Kim et al. [11] have developed an anode-supported flat-tube SOFC by an extrusion process and they report of having obtained 225 mW cm^{-2} at 750 °C. Similar power densities have also been reported by Shao et al. [12] while working on a thermally self-sustaining single-chamber micro SOFC operating on propane, oxygen and helium mixture (helium being the inert). A detailed account of studies that discuss the fabrication of alternative geometries for SOFCs to improve the power density can be found in Singhal and Kendall [13].

In this paper, a different approach is taken to explore the possibility of enhancing the power density of a SOFC. Fig. 1 shows the current density variation along the length of a co-flow SOFC obtained from computations (detailed explanations of how this was obtained are presented later in this paper) at a voltage of 0.73 V. The fuel and the air enter the SOFC system at $x = 0$ and leave the system at $x = 40$ mm. The current density as seen from Fig. 1, decreases from the inlet section to the exit. Similar trends have been observed by Camapanari and Iora [14] while carrying out simulations on planar SOFC. Experimental results on the current density measurements performed by Matti et al. [15] on a polymer electrolyte membrane fuel cell (PEMFC) also indicate a similar variation along the axis of the fuel cell. This aspect can also be understood from the basic Butler–Volmer equations (refer [16]). These equations suggest that the EMF developed is strongly dependent on the partial pressures of the reactants and products. It decreases with the decrease in the partial pressure of the reactants. As one moves from the inlet section of the SOFC towards the outlet in a co-flow arrangement, the reactant mass fraction or its partial pressure continuously decreases due to the consumption of the reactants and production of products in the reaction. The interplay of the above-mentioned factors is depicted in the paper by Yakabe et al. [17]. The decrease in the partial pressure of the reactants due to the consumption of the reactants and production of products in the reaction is essential to the functioning of the SOFC and cannot be done away with. While, there exits a possibility that the decrease in the partial pressure of the reactants due to poor distribution of reactants along the length of the fuel cell could be altered with a different design of the flow channel. The objective of this paper is to explore the possibility of the same.

2. Mathematical model

2.1. Geometry of the fuel cell

CFD ACE commercial package was utilized for the SOFC simulations. The CFD-ACE package discretizes the equations of mass momentum and energy using the finite-volume approach. SIMPLEC (semi-implicit method for pressure-linked equations consistent) [18], a variant of the SIMPLE algorithm [19] is used to solve the discretized in the three-dimensional space. The porous media settings in the package utilizes isotropic linear resistance model (Darcy) with porosity and permeability. The package allows for the electrochemical (Butler–Volmer kinetics) heterogeneous reactions within porous media. The current continuity equations for both the pore phase as well as the solid phase of porous media is solved in the package which facilitates in the accurate determination of the electrode overpotential, necessary to treat electrochemical reactions via Butler–Volmer kinetics. A detailed explanation of the various sub-models of CFD ACE commercial package used in the modeling of SOFC can be found in [20]. The dimensions of the co-flow geometry SOFC used in the present calculations are as shown in Fig. 2. The side view shows the arrangement of anode, cathode, electrolyte and the contacts.

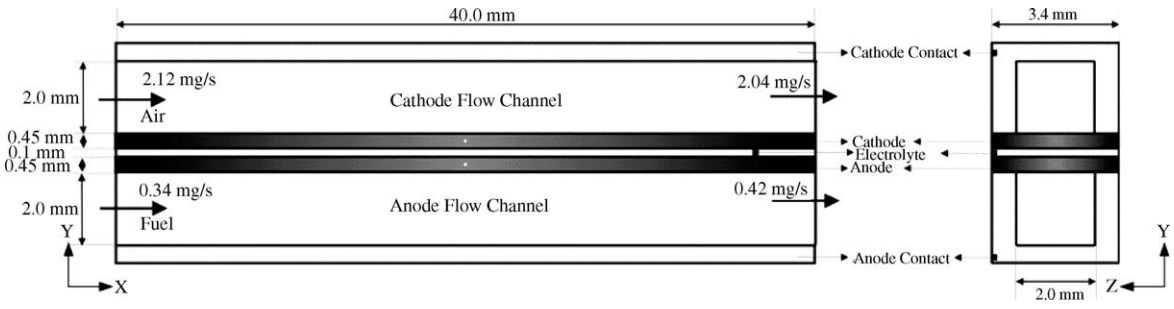

Fig. 2. Schematic of the SOFC used in the calculations along with its various parts and dimensions (not to scale).

Table 1
Porous media settings

Volume name	ε	κ	k	RXN	S/V	Pore	Diffusivity	σ
Anode	0.40	1e–12	6.23	Anode	100	1e–6	Bruggman(2)	100000
Cathode	0.50	1e–12	9.6	Cathode	100	1e–6	Bruggman(2)	7700
Electrolyte	0.01	1e–18	2.7	–	–	1e–6	Bruggman(2)	1e–20

ε: porosity (fluid volume/total volume); κ: permeability (m^2) (total volume/surface area)^2; k: thermal conductivity ($W\,m^{-1}K^{-1}$); S/V: surface to volume ratio (m^{-1}); σ: electrical conductivity ($\Omega^{-1}\,m^{-1}$).

2.2. Materials and property settings

The anode (Ni/ZrO_2 ceramic metal composite (cermet)), cathode (doped lanthanum manganite ($LaMnO_3$)) and electrolyte (yttria-stabilized ZrO_2 (8 mol% Y_2O_3)) are modeled as porous media. The details of the porous media settings are as given in Table 1. The transport properties and conductance used in the current calculations are as given in Table 2. Representative or nominal values have been used here to demonstrate the viability of the idea.

2.3. Chemical reactions

The reactions in the anode and the cathode are modeled as surface reactions and are assumed to take place inside the pores according to the following reaction. The oxygen ions are modeled as "bulk species". The SOFC model used here does not account for internal reforming.

$$\text{anode}: H_2 + CO + 2O^{2-} \rightarrow H_2O + CO_2 + 4e^-$$

$$\text{cathode}: O_2 + 4e^- \rightarrow 2O^{2-}$$

The nominal values for the reference current J_0 and the Tafel constants for the two reactions are as follows:

$$J_0 = 1E + 14, \quad \alpha_a = 0.7, \quad \alpha_c = 0.7 \text{ for anode reaction}$$

$$J_0 = 1E + 10, \quad \alpha_a = 0.7, \quad \alpha_c = 0.7 \text{ for cathode reaction}$$

2.4. Boundary conditions

The inlet mass flow rate into the cathode and the anode flow channels were 2.12×10^{-6} and $3.415 \times 10^{-7}\,kg\,s^{-1}$, respectively. The inlet temperature and pressure into both the flow channels were 1273 K and 1 atm, respectively. At both the cathode and anode outlet, the fixed pressure boundary condition was used and the pressure was 1 atm.

2.5. Grid structure and grid details

The number of grid points utilized in the present study is around 56,000. The typical number of grid points in the x, y and z direction are 80, 70 and 10, respectively. The results were verified to be grid size independent. The calculations are carried out till the residuals associated with all variables decrease by at least 4 orders of magnitude. The time taken for convergence is around 4 h on an Intel 4 PC with 0.5 GB RAM and 2.4 GHz.

3. Results and discussions

The modeling of the flow through a single SOFC was carried out at atmospheric pressure with the CFD-ACE commercial package. The composition of the fuel used was $0.096\,H_2 + 0.428\,H_2O + 0.26\,CO + 0.216\,CO_2$ and air composition was taken as $0.79\,N_2 + 0.21\,O_2$. The composition of the fuel is a typical one obtained from an externally reformed hydrocarbon fuel. In order to verify the computational model, the variation of voltage and power density with the current density (refer Fig. 3) was plotted. The results show a qualitative agreement (similar trend) with those reported in the experimental study by Jiang and Virkar [21], Olga et al. [22] and Sasaki et al. [23]. The maximum power from the SOFC is obtained at around 0.73 V. The calorific value of both hydrogen and carbon monoxide is nearly the same and is around 285 kJ mole^{-1} (see [1]). Using the relationship presented in Larminie and Dicks [16], the maximum possible EMF that can be generated from the SOFC is estimated as 1.48 V. The efficiency of this SOFC at maximum power condition (refer Larminie and Dicks [16]) is around 50%.

Thus having verified the computational model, a thin wall as shown in Fig. 4 was introduced in both the cathode and anode

Table 2
Transport property and conductance settings

Volume Name	ρ	μ	$\sigma(1\,\Omega^{-1}\,m^{-1})$	C_p	k	Γ
Anode	IGL	MixKin	10	JANNAF	MixKin	SCH(0.7)
Cathode	IGL	MixKin	10	JANNAF	MixKin	SCH(0.7)
Electrolyte	IGL	MixKin	10	JANNAF	MixKin	SCH(0.7)
Anode channel	IGL	MixKin	1e–20	JANNAF	MixKin	SCH(0.7)
Cathode channel	IGL	MixKin	1e–20	JANNAF	MixKin	SCH(0.7)

ρ: density ($kg\,m^{-3}$); IGL: ideal gas law; μ: viscosity ($kg\,m^{-1}\,s^{-1}$); MixKin: kinetic theory; σ: electrical conductivity ($\Omega^{-1}\,m^{-1}$); C_p: specific heat ($J\,kg^{-1}\,K^{-1}$) by JANNAF curve fits; k: thermal conductivity ($W\,m^{-1}\,K^{-1}$) and Γ: mass diffusivity ($kg\,m^{-1}\,s^{-1}$) by Schmidt number.

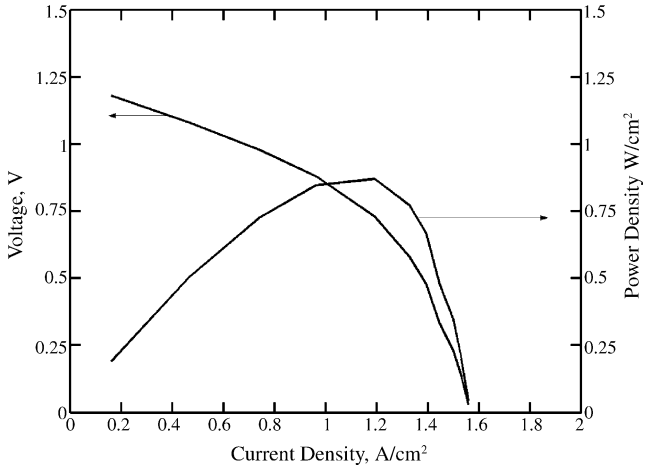

Fig. 3. The polarization characteristics and the power density of a plain geometry SOFC.

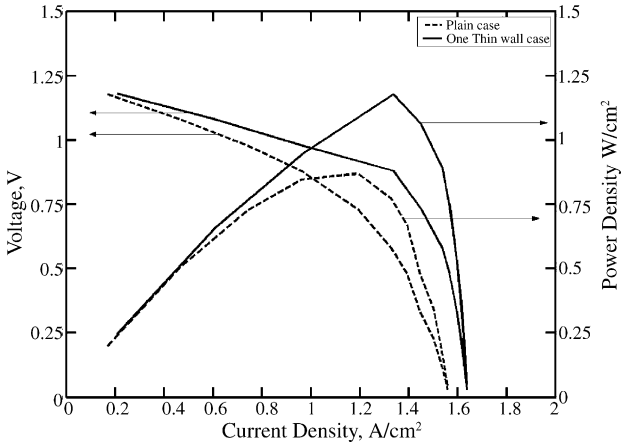

Fig. 5. The polarization characteristics and the power density of both plain and thin-walled geometry SOFC.

flow channel. The purpose of introducing such a thin wall as already been explained in the "Introduction" section is to have an equitable distribution of reactants along the length of the SOFC. It is seen in Fig. 4 that the thin wall runs up to half the length of the fuel cell and that it divides the inlet sections (anode and cathode flow channel) into two halves. Thus, fresh reactants are also made available to the second half (Section II, refer Fig. 4) leading to an even distribution of fresh reactants over the two half lengths (Sections I and II, refer Fig. 4) of the fuel cell.

For the new geometry of the SOFC, the calculations were carried out to obtain the polarization characteristics. The inlet mass flow rates and all other conditions were kept identical for both the plain geometry and the thin-walled geometry. The results of these calculations for both the plain geometry and the thin-walled geometry are as illustrated in Fig. 5. This figure shows the variation of voltage and power density with the current density. It is seen from Fig. 5 that at all voltages the current density obtained from the thin-walled geometry is higher than those obtained with the plain geometry. The improvement in the output power with the thin-walled geometry over the plain geometry can also be observed from Fig. 5. The peak power is obtained with the thin-walled geometry at around 0.88 V, whilst the same with a plain geometry is obtained at 0.73 V. Thus, the efficiency of the SOFC at peak power for the thin-walled geometry, proceeding along lines similar to those outlined in conjunction with Fig. 3 is 60%. The peak power density obtained with the thin-walled geometry is 1.18 W cm^{-2} and the same obtained with a plain geometry is 0.88 W cm^{-2}. The peak power density is around 35% higher with the thin-walled geometry compared to the plain geometry. Thus, with the introduction of the thin wall in the flow channel as shown in Fig. 4, *both the efficiency and the maximum power density of the SOFC were enhanced*. Here, it must be emphasized that the relative improvement in performance of the thin-walled geometry over the plain one is more important than the quantitative values of power density obtained with the two geometries. This method will work when one is constrained to use air and combination of different gases as fuel as is currently used. If hydrogen is used as fuel and oxygen is used as oxidizer, the introduction of thin-walled geometry will not enhance the performance significantly (as reported here) due to the absence of diluants. But in many practical applications, due to cost compulsions and other considerations air, instead of oxygen and a combination of fuels instead of single fuel is used. The introduction of thin-walled geometry in such cases could enhance the performance.

To understand the processes that led to the better performance of the thin-walled geometry compared to the plain geometry, the current density variation along the axis (x) at $y = 0$ and $z = 0$ for

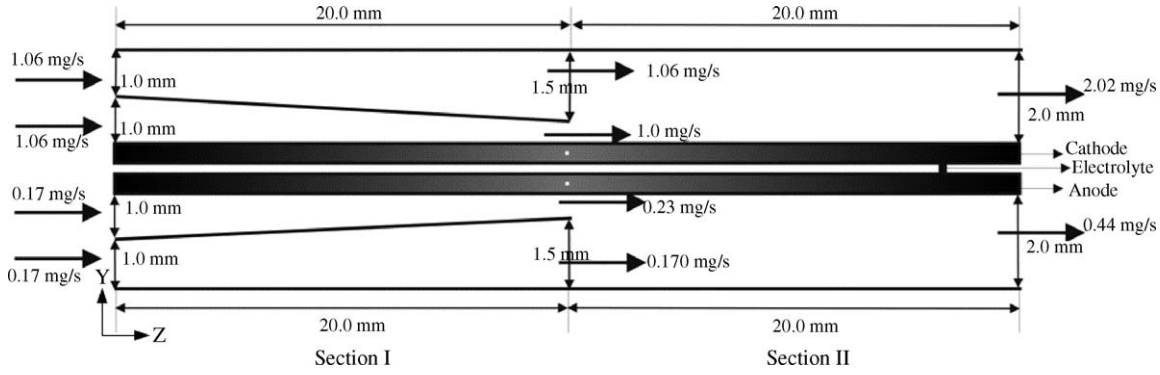

Fig. 4. Schematic of the thin walled geometry SOFC used in the calculations along with the mass flow rates at various locations. The dimensions are as indicated (not to scale).

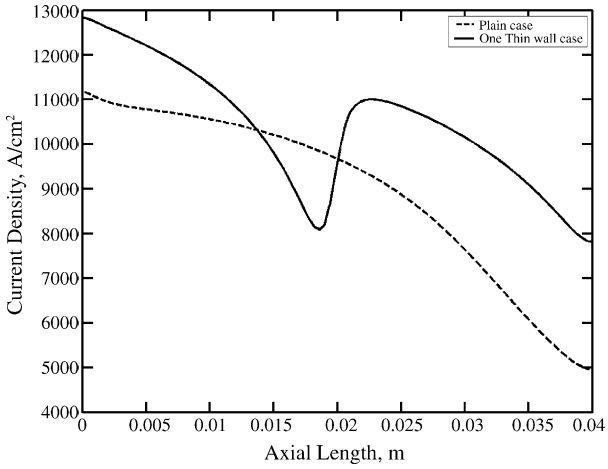

Fig. 6. The current density variation along the axial length of both the plain and thin-walled geometry SOFC at $y = 0$ and $z = 0$ at a voltage of 0.73 V.

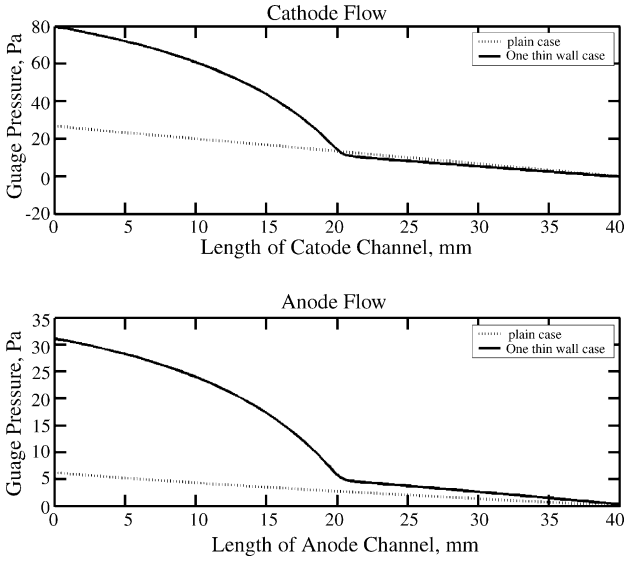

Fig. 7. The pressure distribution along the length of the SOFC close to anode and cathode for both plain and thin-walled geometry at a voltage of 0.73 V.

the two geometries were plotted (refer Fig. 6). The current yield for both geometries from 'Section I' (refer Fig. 4) is almost identical as the area under the two curves are almost the same. The current yield from the second half or 'Section II" (refer Fig. 4) of the SOFC with the thin-walled geometry is higher compared to the plain geometry SOFC. Similar trends were observed at other (y and z) locations too. The increase in the current density in Section II" (refer Fig. 4) of the SOFC with the thin-walled geometry can be attributed to the availability of fresh reactants (explanation to follow later in the paper). Incidentally, if the plain geometry were also to be divided into two halves along its length, then the power density obtained from it's first (nearer to inlet) and second (nearer to outlet) halves are 0.75 and 0.4425 W cm^{-2}, respectively. The corresponding values for the thin-walled geometry are 0.8125 and 0.6375 W cm^{-2}, respectively. The performance of the thin-walled geometry is slightly higher than the plain geometry in the first half, due to the increased mass flux made possible in the thin-walled geometry. The performance of the thin-walled geometry is significantly higher than the plain geometry in the second half. This indicates that the overall enhancement in performance observed with the thin-walled geometry is probably due to the better distribution of reactants to Section II.

The value of current density at $x = 0$ for both geometries are different from each other as can be observed from Fig. 6. This is a rather strange behavior as the initial composition of the fuel and air is identical for both geometries. To understand the reason behind this the pressure plots close to the anode ($y = -0.525$ mm) and cathode ($y = 0.525$ mm) were plotted (refer Fig. 7). It is evident from Fig. 7 that the pressure increases with the introduction of the thin wall in both anode and cathode. From Darcy's law, an increase of pressure near the anode and cathode (both porous media) means increased mass diffusing into anode and cathode. This increased mass flow leads to greater reactions and hence higher current density (at $x = 0$) in the thin-walled geometry.

In order to understand the cause for the improvement in performance of the thin-walled geometry over the plain geometry, the mass fraction profiles of a representative species CO (the largest reactive fuel fraction, CO 26% and H_2 around 10%) were plotted for both the plain geometry and the thin-walled geometry. They are as shown in Fig. 8. It is seen that with the introduction of the thin wall in the flow channel, the distribution of reactants along the length of the flow channel improves significantly. On the basis of Fig. 8, it can be inferred that the improvement in the performance of the thin-walled geometry over the plain ones is due to the more even distribution of reactants along the length of the SOFC.

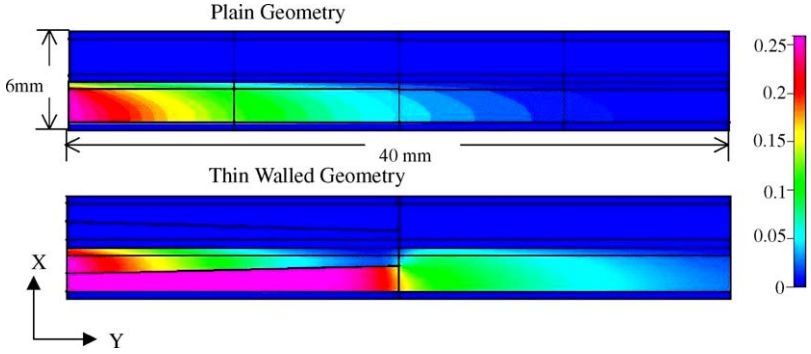

Fig. 8. The mass fraction profiles of CO for both the plain and the thin-walled geometry (Vertical lines are an artifact of the griding procedure only).

Table 3
Current density yields for the thin walled and plain geometries at a voltage of 0.73 V

Factor by which the basic flow has been increased	Current density for the plain geometry, (A cm^{-2})	Current density for the thin-walled geometry, (A cm^{-2})	Improvement of current density with thin-walled geometry (%)
0.5	0.805	0.8625	7
1	1.1925	1.4537	21.9
2	1.5025	1.8538	23.4
4	1.5962	1.9850	24.4
6	1.6187	2.0200	24.8
8	1.6275	2.0375	25.2
10	1.6362	2.0488	25.2

The enhancement in the performance of the SOFC with the thin-walled geometry at a particular inlet flow rate of reactants has been observed. But is this enhancement in performance present at different inlet mass flow rates as well? To address the above question, calculations on the thin-walled geometry and the plain geometry were carried out at different inlet mass flow rates. The results of these calculations are as tabulated in Table 3 for a fixed voltage of 0.73 V. The cathode and the anode mass flow rates of 2.12×10^{-6} and 3.415×10^{-7} kg s^{-1}, respectively were used as the basic unit. The first column in Table 3 gives the factor by which the basic cathode and anode inlet mass flow rates have been simultaneously altered. The last column in Table 3 shows that the performance enhancement obtained with thin-walled geometry over the plain geometry. The performance enhancement with the thin-walled geometry varies from 7–25% over the plain geometry.

At inlet mass flow rates lower than the basic unit (cathode and anode mass flow rates of 1.06×10^{-6} and 1.707×10^{-7} kg s^{-1}, respectively) low levels of improvement (7%) are observed. At these low inlet mass flow rates, the quantity of reactants are lower and they get greater residence time to react as the flow velocities are halved. Hence, a small enhancement (7%) in performance is obtained with the introduction of thin wall. As the inlet mass flow rates are increased to the basic unit and above it, the current densities obtained from the system are also increased (refer column 2 and 3 of Table 3). This is similar to the results reported in literature by Leng et al. [24] and Larrain et al. [25]. At higher inlet mass flow rates, higher current densities (refer column 2 and 3 of Table 3) and in turn higher power densities are obtained. Thus, higher inlet mass flow rates are to be preferred, if enhancing the power density is the objective. At high inlet mass flow rates, the reactant quantity is larger and the accompanied residence time to react is lower. These conditions are quite stringent and call for better flow management of reactants. Hence, with the introduction of the thin wall at high inlet mass flow rates, the improvement in performance of SOFC obtained is significant (22–25%).

4. Conclusions

Three-dimensional simulation of a single SOFC was carried out for two geometries (plain and the thin-walled geometry) using CFD-ACE package. The thin-walled geometry had a thin wall that split the inlet section of both the anode and cathode flow channel into two parts and ran up to half the length of the SOFC. All conditions remaining identical for the two geometries:

(1) The SOFC performance was better with the thin-walled geometry as compared to the plain one due to the better distribution of reactants along the length in the thin-walled geometry.
(2) The thin-walled geometry not only yielded a higher maximum power density of 1.18 W cm^{-2}, but it also led to an improvement in the efficiency at which the maximum power density was obtained (around 60%). For the plain geometry the maximum power density of 0.88 W cm^{-2} was obtained at an efficiency of 50%. The peak power density is around 35% higher with the thin-walled geometry as compared to the plain geometry.
(3) The improvement in the performance of the thin-walled geometry over the plain geometry was small (7%) at low inlet mass flow rates and increased (∼25%) with the increase in inlet mass flow rates.

This research opens up new vistas to explore the possibility of increasing the power density of a SOFC. The results presented here can perhaps be viewed as a logical extension of the desire to have a uniform flow in the fuel cell stacks in order to improve its effectiveness. Although, the results presented here are for a SOFC, they are more generic in nature and can be applied to any other kind of fuel cell. The ideas presented here need to be experimentally authenticated before proceeding further.

Acknowledgment

This work has been partially funded by the Brain Korea 21 project.

References

[1] W. Vielstich, HA. Gasteiger, A. Lamm (Eds.), Handbook of fuel cells, Fundamentals, Technology and Applications 3, vol. I, John Wiley & Sons Ltd, 2003.
[2] A. Bharadwaj, D.H. Archer, E.S. Rubin, Modeling the performance of flattened tubular solid oxide fuel cell, ASME J. Fuel Cell Sci. Technol. 2 (2005) 52–59.
[3] Klaus Hassmann, SOFC power plants, the Siemens–Westinghouse approach, Fuel Cells 1 (2001) 78–84.
[4] P. Lamp, J. Tachtler, O. Finkenwirth, S. Mukerjee, S. Shaffer, Development of an auxiliary power unit with solid oxide fuel cells for automotive applications, Fuel Cells 3 (2003) 146–152.

[5] F.J. Gardner, M.J. Day, N.P. Brandon, M.N. Pashley, M. Cassidy, SOFC technology development at Rolls-Royce, J. Power Sources 86 (2000) 122–129.
[6] Solid State Energy Conversion Alliance, US Department of Energy, www.seca.doe.gov.
[7] P.W. Li, S.P. Chen, M.K. Chyu, "Novel gas distributors and optimization for high power density in fuel cells", J. Power Sources 140 (2005) 311–318.
[8] Sung Pil Yoon, Jonghee Han, Suk Woo Nam, Tae-Hoon Lim, Seong-Ahn Hong, Improvement of anode performance by surface modification for solid oxide fuel cell running on hydrocarbon fuel, J. Power Sources 136 (2004) 30–36.
[9] Takashi Hibino, Hajime Tsunekawa, Satoshi Tanimoto, Mitsuru Sano, Improvement of a single-chamber solid-oxide fuel cell and evaluation of new cell designs, J. Electrochem. Soc. 147 (2000) 1338–1343.
[10] Y. Lu, L. Schaefer, P. Li, Numerical simulation of heat transfer and fluid flow of a flat-tube high power density solid oxide fuel cell, ASME J. Fuel Cell Sci. Technol. 2 (2005) 65–69.
[11] J.H. Kim, R.H. Song, K.S. Song, S.H. Hyun, D.R. Shin, H. Yokokawa, Fabrication and characteristics of anode-supported flat-tube solid oxide fuel cell, J. Power Sources 22 (2003) 138–143.
[12] Z. Shao, S.M. Haile, J. Ahn, P.D. Ronney, Z. Zhan, S.A. Barnett, A thermally self-sustained micro solid-oxide fuel-cell stack with high power density, Nature 435/9 (2005) 795–798.
[13] S.C. Singhal, K. Kendall, High Temperature Solid Oxide Fuel Cells, Elsevier, Amsterdam, 2003.
[14] S. Camapanari, P. Iora, Comparison of finite volume SOFC models for the simulation of a planar cell geometry, Fuel cells 5 (2005) 34–51.
[15] M. Noponen, J. Ihonen, A. Lundblad, G. Lindbergh, Current distribution measurements in a PEMFC with net flow geometry, J. Appl. Electrochem. 34 (2004) 255–262.
[16] James Larminie, Andrew Dicks, Fuel Cell Systems Explained, 2nd ed., John Wiley & Sons, 2003.
[17] H. Yakabe, M. Hishinuma, M. Uratani, Y. Matsuzaki, I. Yasuda, Evaluation and modeling of performance of anode-supported solid oxide fuel cell, J. Power Sources 86 (2000) 423–431.
[18] J.P. Van Doormal, G.D. Raithby, Enhancements of the SIMPLE method for predicting incompressible fluid flows, Numer. Heat Transfer 7 (1984) 147–163.
[19] S.V. Patankar, Numerical Heat Transfer, Hemisphere, Washington DC, 1980.
[20] CFD Research Corp., 2002. CFD-ACE(U)^{TM}User Manual, version 2002. Huntsville, Alabama.
[21] Yi Jiang, Anil V. Virkar, Fuel composition and diluent effect on gas transport and performance of anode-supported SOFCs, J. Electrochem. Soc. 150 (2003) A942–A951.
[22] Olga Costa-Nunes, Raymond J. Gorte, John M. Vohs, Comparison of the performance of Cu–CeO_2–YSZ and Ni–YSZ Composite SOFC Anodes With H_2, CO, and Syngas, J. Power Sources 141 (2005) 241–249.
[23] K. Sasaki, Y. Hori, R. Kikuchi, K. Eguchi, A. Ueno, H. Takeuchi, M. Aizawa, K. Tsujimoto, H. Tajiri, H. Nishikawa, Y. Uchida, Current–voltage characteristics and impedance analysis of solid oxide fuel cells for mixed H_2 and CO gases, J. Electrochem. Soc. 149 (2002) A227–A233.
[24] Y.J. Leng, S.H. Chan, K.A. Khor, S.P. Jiang, Performance evaluation of anode-supported solid oxide fuel cells with thin YSZ electrolyte, Int. J. Hydrogen Energy 29 (2004) 1025–1033.
[25] D. Larrain, J. Van herle, F. Maréchal, D. Favrat, Generalized model of planar SOFC repeat element for design optimization, J. Power Sources 131 (2004) 304–312.